MATERIALS SCIENCE

Giant Rashba splitting in 2D organic-inorganic halide perovskites measured by transient spectroscopies

Yaxin Zhai,[1]* Sangita Baniya,[1]* Chuang Zhang,[1] Junwen Li,[2,3] Paul Haney,[2] Chuan-Xiang Sheng,[1,4†] Eitan Ehrenfreund,[1,5] Zeev Valy Vardeny[1†]

Two-dimensional (2D) layered hybrid organic-inorganic halide perovskite semiconductors form natural "multiple quantum wells" that have strong spin-orbit coupling due to the heavy elements in their building blocks. This may lead to "Rashba splitting" close to the extrema in the electron bands. We have used a plethora of ultrafast transient, nonlinear optical spectroscopies and theoretical calculations to study the primary (excitons) and long-lived (free carriers) photoexcitations in thin films of 2D perovskite, namely, $(C_6H_5C_2H_4NH_3)_2PbI_4$. The density functional theory calculation shows the occurrence of Rashba splitting in the plane perpendicular to the 2D barrier. From the electroabsorption spectrum and photoinduced absorption spectra from excitons and free carriers, we obtain a giant Rashba splitting in this compound, with energy splitting of (40 ± 5) meV and Rashba parameter of (1.6 ± 0.1) eV·Å, which are among the highest Rashba splitting size parameters reported so far. This finding shows that 2D hybrid perovskites have great promise for potential applications in spintronics.

INTRODUCTION

The extrema points in the conduction band (CB) and valence band (VB) of semiconductors are of utmost importance in determining the optical, spin, and transport properties of these materials. The electron dispersion relation, $E(k)$, near these extrema points is usually described by the effective-mass approximation, where the electrons and holes are treated as "free carriers" having an effective mass, m^*, that leads to a spin-degenerate parabolic dispersion, $E(k) = \hbar^2k^2/2m^*$ (Fig. 1A). However, spin-orbit coupling (SOC) can split the spin-degenerate bands in noncentrosymmetric compounds, as first realized by Dresselhaus *et al.* (*1*) and Rashba (*2*). The effect of SOC may be enhanced in reduced dimensions, such as in two-dimensional (2D) semiconductors (*3*). In the presence of structural "inversion asymmetry," the spin-degenerate parabolic band splits into two spin-polarized bands, where the electron (or/and hole) dispersion relation may be described by $E_{\pm}(k) = (\hbar^2k^2/2m^*) \pm \alpha_R|k|$, where α_R is the Rashba splitting parameter. This formulation yields new extrema at a momentum offset (k_0) and energy splitting (E_R) that are related to each other via $\alpha_R = 2E_R/k_0$ (Fig. 1B) (*4*). The two Rashba split branches have opposite spins, which can influence the photoexcitation's optical and magnetic properties, a situation that may benefit spintronics because it enhances the spin-to-charge conversion efficiency (*4*, *5*).

Large Rashba splitting with α_R of few electron volt angstrom has been observed in only a handful of materials (such as ultrathin metallic films) (*6*), surfaces of topological insulators (such as Bi_2Se_3) (*7*), and surfaces of the polar semiconductor BiTeI (*8*). We note that Rashba splitting is very small in traditional III-V semiconductors. For example, the Rashba splitting parameter α_R at the interface of InAlAs/InGaAs was measured to be ≈0.07 eV·Å with $E_R \approx 1$ meV (*9*). In contrast, here, we discovered a giant-sized Rashba splitting in a 2D semiconducting layered hybrid organic-inorganic perovskite.

The 3D hybrid organic-inorganic perovskites (thereafter, hybrid perovskites), such as methyl ammonium lead halogen ($MAPbX_3$, where X is a halogen), have recently attracted immense attention because of several promising optoelectronic device applications, such as photovoltaic solar cells, light-emitting diodes, and lasers (*10*, *11*). These compounds have strong SOC due to the heavy elements (Pb, X) that determine the electron bands near their extrema points, which may lead to large Rashba splitting if the structure lacks inversion symmetry (*12*); this is realized in some 2D and 3D hybrid perovskites (*13*). Interest in the hybrid perovskites for spintronics applications has only recently begun, with promising spin and magnetic field phenomena (*14*, *15*); therefore, solid evidence of Rashba splitting existence in these compounds would further boost this interest.

Recently, the 2D hybrid perovskites have come into focus (*16*, *17*). These compounds self-assemble into alternating organic and inorganic layers that form natural "multiple quantum wells," with outstanding optoelectronic characteristics and stability under ambient conditions. Having strong SOC, high charge mobility, and intrinsic quantum well structures with many interfaces and facile solution processability, the 2D hybrid perovskites may be promising candidates for room temperature spintronic applications (*18*). Our work shows that these materials may also exhibit giant Rashba splitting, which could further enhance their appeal for this field.

RESULTS

We have used a variety of transient and steady-state linear and nonlinear optical spectroscopies, as well as theoretical calculations to study the optical characteristics of the primary (excitons) and long-lived (free carriers) photoexcitations in 2D hybrid perovskite films (see the Supplementary Materials). Figure 1C schematically shows the 2D hybrid perovskite that we studied here, namely, $(C_6H_5C_2H_4NH_3)_2PbI_4$ (PEPI), where the organic ($C_6H_5C_2H_4NH_3^+$) and inorganic $[PbI_6]^{4-}$ octahedron layers form multiple quantum wells with thickness of ≈1 nm (barrier) and ≈0.6 nm (well), respectively (*19*). A detailed description that includes energy gaps of the respective wells and barriers is given in fig. S1. The spectroscopies and model calculations used in this work, as

[1]Department of Physics and Astronomy, University of Utah, Salt Lake City, UT 84112, USA. [2]Center for Nanoscale Science and Technology, National Institute of Standards and Technology, Gaithersburg, MD 20899, USA. [3]Maryland NanoCenter, University of Maryland, College Park, MD 20742, USA. [4]School of Electronic and Optical Engineering, Nanjing University of Science and Technology, Nanjing 210094, China. [5]Physics Department and Solid State Institute, Technion-Israel Institute of Technology, Haifa 32000, Israel.
*These authors contributed equally to this work.
†Corresponding author. Email: val@physics.utah.edu (Z.V.V.); cxsheng@njust.edu.cn (C.-X.S.)

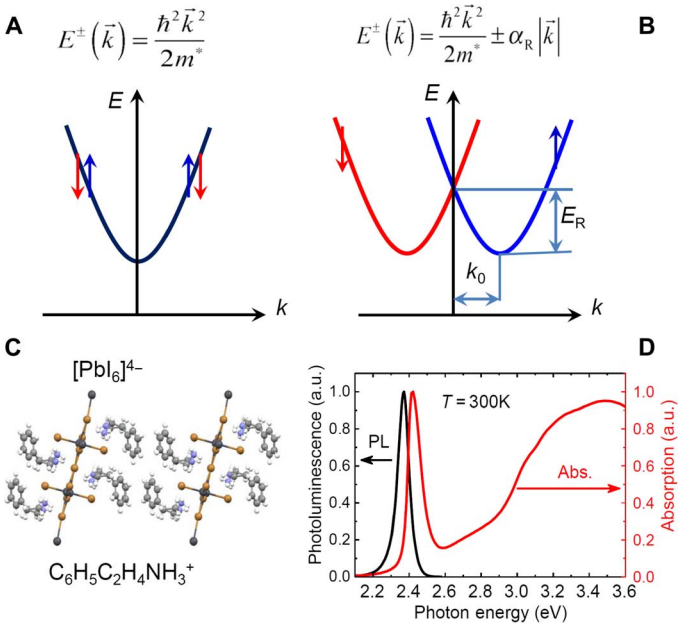

Fig. 1. Introduction to Rashba splitting and the 2D layered hybrid perovskite PEPI. (**A**) Schematic electron dispersion relation of a regular CB that shows a doubly spin-degenerate parabolic band having a single minimum at $k = 0$. (**B**) Same as in (A) but subjected to Rashba splitting; two parabolic branches having opposite spin sense are formed. The Rashba energy (E_R) and momentum offset (k_0) are denoted. (**C**) Structure of PEPI having alternating organic ($C_6H_5C_2H_4NH_3^+$) and inorganic $[PbI_6]^{4-}$ layers that form multiple quantum wells. (**D**) Absorption (Abs) and PL spectra of PEPI film at room temperature. a.u., arbitrary units.

detailed in Materials and Methods, provide compelling evidence that the continuum band edge above the exciton level (CB bottom and/or VB top) has surprising optical characteristic properties, which result from a large Rashba splitting energy, $E_R \approx 40$ meV. Our work provides a general all-optical method to study the Rashba splitting effect in semiconductors.

The room temperature photoluminescence (PL) and absorption spectra of the 2D hybrid perovskite PEPI film are dominated by an exciton band at ≈2.4 eV with large oscillator strength, consistent with a relatively large exciton binding energy, $E_B \approx 0.2$ eV (Fig. 1D) (*20*), followed by a slow increase in the absorption with an onset at ≈2.6 eV. However, at low temperatures ($T < 110$ K), the absorption spectrum shows two step-like absorption edges in the spectral range of 2.45 to 2.65 eV (Fig. 2A and fig. S2). We thus used a modulation spectroscopy, namely, the electroabsorption (EA), to separate these delicate absorption features from the broad spectral background. Recall that the EA spectrum in neat semiconductors having intermediately large E_B usually contains two different spectral features: a Stark shift of the exciton below the continuum and a Frank-Keldysh (FK)–type oscillatory feature at the continuum band edge (*21*).

Figure 2B shows low-temperature EA spectra of the PEPI obtained at various ac field strengths. On the basis of the EA dependence on the field strength (or V, the applied voltage), we identify two distinctive EA spectral ranges. The EA scales with V^2 (fig. S3) for $\hbar\omega < 2.55$ eV (*22*), but it saturates at large field for $\hbar\omega > 2.55$ eV (Fig. 2D, inset). The EA spectrum in the low-energy spectral region (<2.55 eV) shows a "first derivative–like" feature consistent with an exciton Stark shift, having a zero crossing at 2.38 eV that we assign as the 1s exciton energy, E_{1s} (Fig. 2F). We note that in this spectral region, there is a second derivative–like feature with "trending" zero crossing at ≈2.53 eV, in agreement with the lowest step-like feature in the absorption spectrum (Fig. 2A). We identify this EA feature as originating from the 2s exciton in PEPI (*23*) instead of another exciton series (*24*), as shown in Fig. 2F (*13*, *25*).

In contrast, the large oscillatory-like EA feature at $\hbar\omega > 2.55$ eV having multiple zero crossings is due to FK oscillation above the direct band edge (*21*, *26*). The oscillation energy period δE shows "field broadening" that scales with $V^{2/3}$ (Fig. 2, C to E). This broadening and the EA saturation at large V are typical characteristic properties of the FK oscillation in the EA spectrum close to the band edge [interband (IB) transition in Fig. 2B], where the peak at energy below the first zero crossing determines the energy gap value. We thus locate the band edge of the PEPI film at 2.57 eV (Fig. 2B). From E(IB), E_{1s}, and E_{2s}, we can now obtain the 1s and 2s exciton binding energies, $E_B(1s) = (190 \pm 4)$ meV and $E_B(2s) = (45 \pm 8)$ meV, respectively. The uncertainty originates mainly from the optical resolution of our spectrometer (2-nm entrance slit size) and the film inhomogeneity; all uncertainties are reported as 1 SD.

To further investigate the excited-state properties of PEPI close to the continuum band minima, we studied the primary photoexcitations using the picosecond transient photomodulation (PM) with 250-fs time resolution in a broad spectral range of 0.23 to 2.8 eV, excited at 3.1 eV (see Materials and Methods). The PM spectrum contains photoinduced absorption (PA) bands with $\Delta T < 0$ due to excited-state absorption and photoinduced bleaching (PB), with $\Delta T > 0$ caused by pump-induced bleaching of the ground-state absorption. At $t = 0$ ps, the PM spectrum contains two dominant spectral features (Fig. 3A): a PA band in the mid-infrared (IR) spectral range, denoted as PA_1 at ≈0.35 eV, and a PM feature in the visible spectral range centered at the PEPI exciton absorption (≈2.4 eV) having both PA and PB components, as well as a weak PA band at ≈1 eV denoted as PA_2. We note the occurrence of "zero sum" when adding the PA and PB bands of the entire PM spectrum, indicating that there are no other important photoinduced features in the spectrum. In addition, the PA and PM bands share similar decay dynamics (Fig. 3B), which supports the notion that they originate from a single primary photoexcitation species. We note that the PB dynamics contain a much slower component that is represented by a constant in the decay fitting (Fig. 3B), indicating that some long-lived photoexcitations survive the fast exciton recombination; these may be photocarriers, as discussed below.

The PM band in the visible range can be fit by linear combination of PB of the absorption spectrum and the absorption first and second derivatives, as shown in fig. S4. Therefore, it can be explained by a combination of "band filling" due to the primary photoexcitation (*27*), photoinduced symmetry-breaking process [such as spatially inhomogeneous strain or photoinduced electric field (*18*, *28*)], and transient broadening (*29*). From the exciton PB in the PM spectrum and strong PL emission from PEPI (Fig. 1D), we conclude that the primary photoexcitations in this 2D perovskite are excitons, mainly 1s excitons. We can therefore study the electron bands simply from the exciton transition into the adjacent continuum band(s), as schematically depicted in Fig. 3C.

The PA_1 band from the excitons into the continuum band peaks at (350 ± 2) meV (the uncertainty comes from the 150-fs pulse duration), which cannot be ascribed to the vertical transition from the 1s exciton into the lowest continuum band because from our EA studies, a transition into the lowest continuum band should appear at 190 meV. We therefore assign PA_1 to an optical transition from the 1s exciton to a

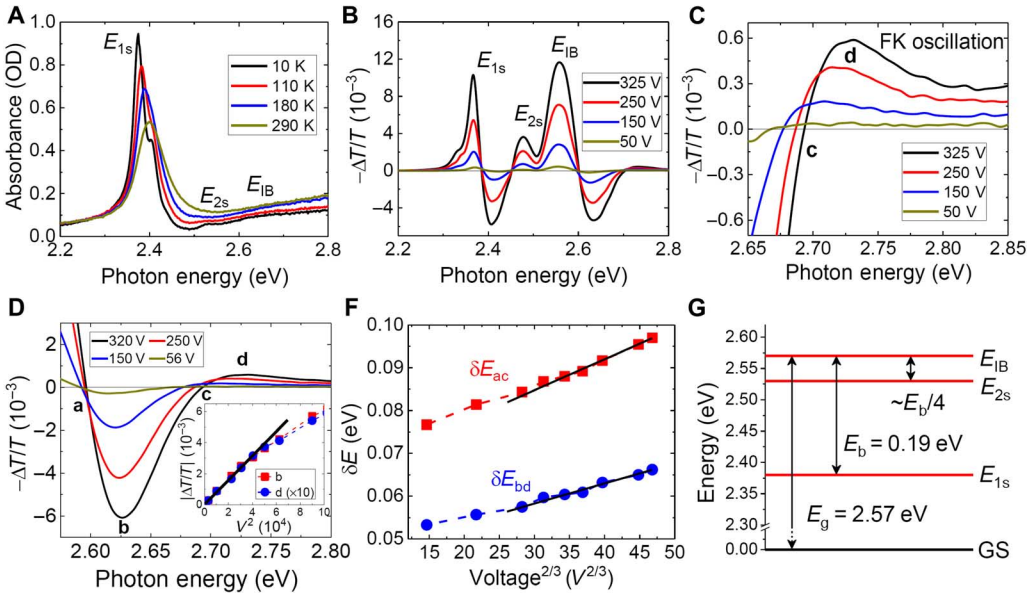

Fig. 2. Absorption and EA spectra of PEPI film. (**A**) Absorption spectra of PEPI film at various temperatures. The 1s and 2s exciton (E_{1s} and E_{2s}, respectively) and an IB transition are assigned. OD, optical density. (**B**) EA spectra of PEPI measured at 45 K at various applied electric fields (the applied voltage, *V*). Various EA spectral features are assigned. (**C**) EA spectra close to the zero-crossing energy "c" measured at various field strengths; broadening of the FK oscillation is seen. "c" represents zero crossing energies, and "d" represents the high-energy FK oscillation that blueshifts with increasing field. (**D**) Field broadening of the EA features related to the FK oscillation; "a," "b," "c," and "d" are assigned as zero-crossing energies and peak positions, respectively. The inset shows the peak values of EA versus V^2 of bands b and d, which saturate at large *V*. (**E**) Energy differences δE_{ac} and δE_{bc} plotted versus $V^{2/3}$. (**F**) Energy levels of the excitons (E_{1s} and E_{2s}) and interband transition [*E*(IB)] are assigned with respect to the ground state (GS).

second, upper electron continuum branch, which is split from the lower band by Rashba SOC, as shown schematically in Fig. 3C. We have looked for a second PA band at ≈0.2 eV (that is, into the lower continuum band) but could not find any hint of it down to 0.23 eV (Fig. 3A, inset). Our finding suggests that a direct optical transition from the exciton into the lower Rashba split branch is either forbidden or much weaker compared to that in traditional semiconductors such as GaAs (*30*). To rationalize this result, we note that the transition from a 1s exciton to a band minimum of free electron–hole pairs is proportional to the electrical dipole moment matrix element between a CB (or VB) state and itself. This is because the initial exciton includes a Bloch state of the CB minimum, and the final electron–hole pair includes this same Bloch state. This matrix element is nothing more than the momentum expectation value of the Bloch state, which vanishes at the band minimum. In previous analysis of the exciton-CB transition in GaAs (*30*), the authors replaced the free carrier wave function by a p-state of an unbound electron–hole pair wave function, enabling the dipole transition exciton→continuum band. In our 2D perovskite film, disorder from point defects and grain boundaries may destroy the coherence of the unbound electron–hole pair, so that optical transitions rely solely on the properties of the Bloch wave functions. Figure 4D shows the density functional theory (DFT) calculation of various electrical dipole transition matrix elements, which verifies that only transitions into the upper Rashba split CB are allowed (see the Supplementary Materials).

We can now obtain the Rashba splitting energy, E_R, from the PA_1 band at 350 meV, because PA_1 should be pushed to higher energies by an energy, $\Delta E = 4E_R$, namely, $E(PA_1) = E_B+4E_R$ (Fig. 3C). Using this relation, E_B (=190 meV from the EA spectrum) and $E(PA_1) = 350$ meV (from the transient PA spectrum), we determine $E_R = (40 \pm 5)$ meV in 2D PEPI. We note that the PA_1 spectrum is asymmetric; this may be due to the transition from the exciton discrete level to the continuum band, where the exciton wave function is spread in *k*-space by a "*k*-localization length," Δk, as determined by its localization length *l* in real space and $\Delta k \approx 1/l$ (see discussion in the Supplementary Materials) (*18*). In the inset of Fig. 3A, the solid line through the PA_1 data points is a fit using the optical transition model for a 2D semiconductor described in eq. S4 (see the Supplementary Materials), from which we obtain the exciton localization length $l \approx 10$ nm (see the Supplementary Materials). This relatively large *l* value indicates that the exciton is quite delocalized in the quantum well in a direction perpendicular to the barriers but localized in *k*-space. In addition, the weak PA_2 band at ≈1 eV may be readily explained as the optical transition from the exciton level at ≈2.4 eV into higher-lying bands at ≈3.3 eV, which can be seen in the absorption spectrum (fig. S2), similar to the transient PM spectra of excitons in nanotubes and in $CH_3NH_3PbI_3$ (*31*).

Furthermore, we expect that the presence of Rashba splitting would affect the process that leads to free carrier absorption (FCA). To investigate this assumption, we studied the properties of long-lived photoexcitations in PEPI using the technique of steady-state PM (see Materials and Methods). The long-lived photoexcitations should be free carriers because the excitons have a sufficiently long time to ionize into free electrons and holes that can contribute to photocarriers, especially at grain boundaries. This has been verified in PV cells based on 2D perovskites that have shown power conversion efficiency larger than 10% (*16*). In this case, the PM spectrum would be due to photogenerated FCA.

To verify that we can measure photoinduced FCA by our PM technique, we measured, as a "control experiment," the steady-state PM spectrum in crystalline Si at 45 K, as seen in Fig. 5A. We could readily fit this PA spectrum by a Drude-type FCA response, in which the PA spectrum varies as ω^{-2} (*32*); this validates our approach. In contrast, the steady-state PA spectrum (PA_{FCA}) in PEPI film shows a sharp dip at low photon energy, forming a peak at $\hbar\omega \approx 0.15$ eV. We consider this surprising FCA(ω) response as a "smoking-gun" verification of the

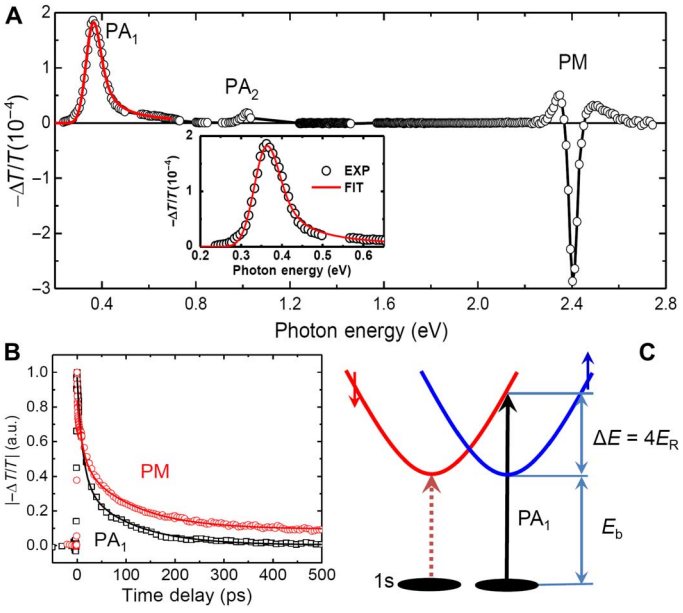

Fig. 3. Ultrafast PM spectroscopy of PEPI film excited at 3.1 eV. (**A**) PM spectrum at t = 0 ps; PA_1, PA_2, and PM are assigned. The solid line through the data points of PA_1 shown in the inset is a fit using a theoretical model for the exciton transition into the continuum (see main text and the Supplementary Materials). (**B**) Decay dynamics of the PM band at 2.4 eV and PA_1 at 0.36 eV up to 500 ps. The lines through the data points are fits using double exponential decay ($A_1e^{-t/t1} + A_2e^{-t/t2} + C$), where t_1 = 11.9 and 11.8 ps, t_2 = 103 and 108 ps, and C = 0.003 and 0.094 for the PA_1 and PM bands, respectively. (**C**) Schematic energy diagram with Rashba splitting that explains the PA_1 transition. The Rashba energy (E_R) may be obtained from the one-quarter of energy difference (ΔE) between PA_1 transition and the 1s exciton binding energy (E_b).

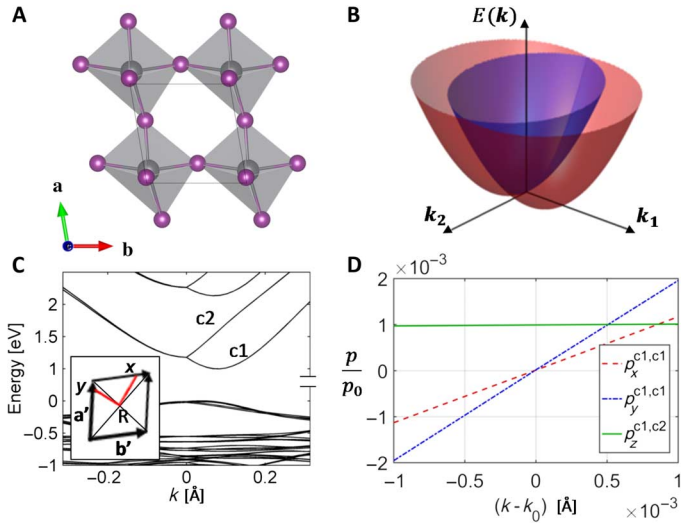

Fig. 4. DFT calculations on the 2D perovskite. (**A**) One layer of the Pb-I octahedra that describes the relaxed structure of the PEPI used in the DFT calculations. The Pb atom (gray sphere) is displaced from the octahedra center along the **a** + **b** direction, which breaks off the inversion symmetry, resulting in Rashba splitting caused by SOC. The unit cell vectors **a** and **b** lie in the x-y plane with an angle of 99.7° between them. (**B**) Schematic of the CB energy dispersion near the R point in the Brillouin zone, where $\mathbf{k}_{1(2)}$ is directed along the **a** +(−) **b** direction. (**C**) Electronic band structure near the R point, which shows the Rashba splitting along a direction perpendicular to the symmetry-breaking direction; c1 and c2 represent the lower and upper Rashba bands, respectively. (**D**) DFT-calculated momentum matrix elements versus k near the band minimum (at k_0 = 0.07 Å^{-1}) away from the R point along the (1, −1) direction. Red and blue lines correspond to x and y component of the momentum matrix element between lowest CB c1 and itself, showing the vanishing transition between the exciton and lowest Rashba split CB at $k = k_0$. The green curve is the z component of the momentum matrix element between the Rashba split bands c1 and c2, which is nonzero for all k. The y axis is dimensionless, with the computed momentum p presented in terms of its value in Rydberg units: $p_0 = 1.99 \times 10^{-24}$ kg/(m·s).

Rashba splitting that exists in the PEPI continuum band. Because optical transitions within the same branch can only be Drude-like, which is allowed because of the mixture of s-state and p-state in the CB (see the Supplementary Materials), we ascribe this PA band to FCA with an onset at the vertical transition from the bottom of one branch of the CB into the other branch, as shown schematically in Fig. 5B. This transition is allowed because it involves states of nonzero k-value for the upper and lower spin-split branches of the CB and, therefore, a mixture of s-state and p-state (see details in the Supplementary Materials).

The obtained FCA peak at 0.15 eV agrees with the optical transition of the excitons (PA_1) measured by the picosecond transient PM (Fig. 3A) because both transitions contain an "add-on" energy, $\Delta E = 4E_R$ (Figs. 3D and 5B). From the FCA peak at 0.15 eV, we obtain Rashba splitting energy, $E_R \approx (38 \pm 3)$ meV. Another source of uncertainty in this measurement is the unknown value of the quasi-Fermi level at the CB bottom, which may well be of order of 2 to 3 meV at low temperature. We therefore conclude that the FCA results agree with $E_R = (40 \pm 5)$ meV determined from the transient picosecond spectroscopy.

From the obtained E_R value, we can readily estimate the offset, k_0, in the momentum space using a parabolic dispersion relation with an electron effective mass obtained using DFT $m^* = 0.25m_0$ (where m_0 is the bare electron mass); we thus obtained $k_0 = (0.051 \pm 0.004)$ Å^{-1}. Consequently, we estimate that the Rashba splitting parameter $\alpha_R = (1.6 \pm 0.1)$ eV·Å. These values are comparable to the recently measured Rashba parameters in $MAPbBr_3$ using the surface-sensitive angle-resolved photoelectron spectroscopy (*33*).

To help understand the origin of the Rashba spin-orbit splitting of the CB, we carry out first-principles DFT calculations using local density approximation (LDA) in the form of ultrasoft pseudopotentials, as implemented using Quantum ESPRESSO (see the Supplementary Materials). Figure 4A shows the geometry of the relaxed structure. We find that the inversion symmetry is broken due to the Pb atom displacement from the octahedral center. The displacement is in the 2D plane, roughly in the direction of **a** + **b**, where **a** and **b** are the in-plane lattice vectors. This leads to the Rashba band splitting for states with crystal momentum oriented perpendicularly to the symmetry-breaking direction, as shown in Fig. 4C. The dashed red and blue lines in Fig. 4D show the optical transition matrix elements within the lowest CB, which, as discussed above, vanish at the minimum of the energy dispersion. The solid green line denotes the IB matrix element, which does not vanish at this point, indicating that the optical transition is allowed. An effective tight-binding model given in the Supplementary Materials shows that the source of this optical transition is sp-hybridization present in the CB eigenstates at the band minimum. From our model calculation, we obtain band splitting energy, E_R = 160 meV, which is larger than the experimentally determined splitting. We attribute this discrepancy to approximations used in LDA. For more quantitatively accurate description of the electronic structure, a calculation at the level of quasi-particle GW is likely required.

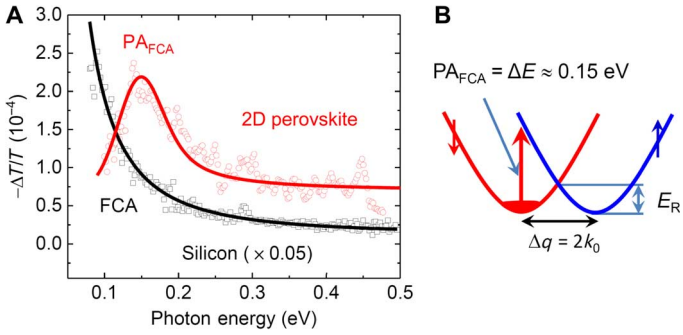

Fig. 5. Steady-state PM spectroscopy of PEPI film excited at 2.8 eV. (**A**) PM spectrum of PEPI film compared to that of a silicon wafer measured at modulation frequency of 350 Hz and temperature of 45 K. The PA bands, PA_{FCA} for PEPI and FCA for Si, are assigned. The solid lines through the data points are fits using the Drude model (PA, $\sim\omega^{-2}$) for the Si wafer and eq. S4 for the PEPI (see the Supplementary Materials). (**B**) Schematic electron energy bands with Rashba splitting that explain the FCA in PEPI. The Rashba energy (E_R) and momentum offset ($k_0 = \Delta q/2$) are assigned.

DISCUSSION

In conclusion, strong spin-orbit coupling in the 2D perovskite PEPI causes Rashba splitting in the continuum band, where the spin-degenerate parabolic band splits into two branches with opposite spin-aligned electronic states. This causes both the optical transitions of excitons into the continuum band and FCA within the continuum band to acquire an add-on energy term of $4E_R$. From the peak of the exciton transition measured by picosecond transient PM and the FCA measured by steady-state PM, we have determined the Rashba splitting energy, $E_R = (40 \pm 5)$ meV in PEPI 2D hybrid perovskite, which is among the highest values reported so far. Our work provides a comprehensive, all-optical method to study the Rashba splitting effect in semiconductors.

MATERIALS AND METHODS

Sample preparation

The 2D hybrid perovskite films were fabricated in a nitrogen-filled glove box with oxygen and moisture levels of <1 part per million. We mixed R-NH_3I (where R was $C_6H_5C_2H_4$) and PbI_2 in a 2:1 mole ratio in *N*,*N*′-dimethylformamide to form solutions with a concentration of 0.5 mol/ml. The solutions were spin-coated on an oxygen plasma–pretreated sapphire or KBr substrates at 420 rad/s and 90 s to form 100-nm thick films; the obtained films were subsequently annealed at 100°C for 30 min. The purchased chemicals were used without further purification. From the high transmission through the film and the observation of numerous diffraction orders (fig. S2), we concluded that our spectroscopies were performed on high-quality films.

Transient PM spectroscopy

The main technique in the present study for measurement of the primary photoexcitation in the 2D hybrid perovskites was transient PM spectroscopy using the pump-probe correlation method. In this technique, the pump pulse excites the sample, and the mechanically delayed probe pulse measures the pump-induced changes, $\Delta T(t)$, in the sample transmission T. The PM spectrum contains PA bands with $\Delta T < 0$ due to excited-state absorption and PB with $\Delta T > 0$ caused by pump-induced bleaching of the ground-state absorption. We used two laser systems based on a Ti:Sapphire oscillator: a low-power (energy per pulse ≈ 0.1 nJ) high repetition rate (≈80 MHz) laser for the mid-IR spectral range and a high-power (energy per pulse ≈10 μJ) low repetition rate (≈1 kHz) laser for the near-IR/visible spectral range. The pump excitation for both laser systems was set at $\hbar\omega = 3.1$ eV. For the low-intensity measurements in the mid-IR spectral range, we used an optical parametric oscillator (Opal, Spectra-Physics) that generates $\hbar\omega$ (probe) from 0.25 to 1.05 eV; for the high-intensity measurements, white-light supercontinuum was generated for $\hbar\omega$ (probe) ranging from 1.15 to 2.7 eV. The transient PM spectra from the two laser systems were normalized to each other using the fundamental (1.55 eV) probe from the low-power laser system. For the PM spectrum in the visible spectral range, we used a Si photodiode, whereas for the mid-IR spectral range, we used an InSb photodiode that was cooled to 80 K to minimize the dark electrical noise.

EA measurements

We used a 2D perovskite film fabricated on a substrate with patterned metallic electrodes. The EA substrate consisted of two interdigitated sets of a few hundreds of 10-μm-wide gold electrodes, which were patterned on a sapphire substrate. The device was placed in a cryostat for low-temperature measurements. By applying a potential, V, to the electrodes, a typical electric field, $F \approx 10^5$ V/cm, was generated, with $V = 300$ V and $f = 1$ kHz parallel to the film. To probe the EA spectrum, we used an incandescent light source from a Xe lamp, which was dispersed through a monochromator, focused on the sample, and detected by an ultraviolet-enhanced silicon photodiode. We measured the changes, ΔT, in the transmission spectrum T using a lock-in amplifier, set to twice the frequency ($2f$) of the applied field, and verified that no EA signal was observed at f or $3f$. ΔT and T spectra were measured separately using a Si photodiode, and the EA spectrum was obtained from the ratio $\Delta T/T$.

Continuous-wave PM measurements

The excitation pump was provided by a diode laser with $\hbar\omega = 2.8$ eV, and the probe beam was provided by an incandescent tungsten/halogen lamp (for the visible/near-IR) or a globar light source (for mid-IR). The sample films grown on KBr substrates were put in a cryostat under vacuum. The sample temperature was varied from 50 to 300 K. The pump and probe beams were overlapped on the sample films, and the transmitted probe beam was filtered through a monochromator and detected by a Si, InGaAs, or HgCdTe detector for different probe spectral ranges. The transmission T and the change of the transmitted probe beam (ΔT), which was caused by the modulated pump beam, were detected by a lock-in amplifier. The PA spectrum was then calculated from $\Delta T/T$.

SUPPLEMENTARY MATERIALS

Supplementary material for this article is available at http://advances.sciencemag.org/cgi/content/full/3/7/e1700704/DC1

Supplementary Text

Fitting the PA_1 band at $t = 0$ ps shown in Fig. 3A

Inter-Rashba optical transitions in 2D perovskites

DFT calculations

Fitting the PA_{FCA} band shown in Fig. 5A

fig. S1. Schematic structure of PEPI with alternating organic and inorganic layers, forming multiple quantum wells onto the substrate.

fig. S2. The absorption spectrum of a PEPI film measured at temperatures ranging from 10 to 290 K, as denoted.

fig. S3. The dependence of the EA signal on V^2 at various energies below the IB edge at 2.55 eV, where V is the applied voltage.

fig. S4. The transient PM band of PEPI film measured at t = 0 ps and 300 K and its fit using a linear combination of the absorption spectrum and its first and second derivatives.
References (*34*–*38*)

REFERENCES AND NOTES

1. G. Dresselhaus, A. F. Kip, C. Kittel, Spin-orbit interaction and the effective masses of holes in germanium. *Phys. Rev.* **95**, 568–569 (1954).
2. E. I. Rashba, Properties of semiconductors with an extremum loop. 1. Cyclotron and combinational resonance in a magnetic field perpendicular to the plane of the loop. *Phys. Solid State* **2**, 1224–1238 (1960).
3. Y. A. Bychkov, E. I. Rashba, Properties of a 2D electron gas with lifted spectral degeneracy. *JETP Lett.* **39**, 78–81 (1984).
4. A. Manchon, H. C. Koo, J. Nitta, S. M. Frolov, R. A. Duine, New perspectives for Rashba spin-orbit coupling. *Nat. Mater.* **14**, 871–882 (2015).
5. E. Lesne, Y. Fu, S. Oyarzun, J. C. Rojas-Sánchez, D. C. Vaz, H. Naganuma, G. Sicoli, J.-P. Attané, M. Jamet, E. Jacquet, J.-M. George, A. Barthélémy, H. Jaffrès, A. Fert, M. Bibes, L. Vila, Highly efficient and tunable spin-to-charge conversion through Rashba coupling at oxide interfaces. *Nat. Mater.* **15**, 1261–1266 (2016).
6. E. Frantzeskakis, S. Pons, H. Mirhosseini, J. Henk, C. R. Ast, M. Grioni, Tunable spin gaps in a quantum-confined geometry. *Phys. Rev. Lett.* **101**, 196805 (2008).
7. P. D. C. King, R. C. Hatch, M. Bianchi, R. Ovsyannikov, C. Lupulescu, G. Landolt, B. Slomski, J. H. Dil, D. Guan, J. L. Mi, E. D. L. Rienks, J. Fink, A. Lindblad, S. Svensson, S. Bao, G. Balakrishnan, B. B. Iversen, J. Osterwalder, W. Eberhardt, F. Baumberger, P. Hofmann, Large tunable Rashba spin splitting of a two-dimensional electron gas in Bi_2Se_3. *Phys. Rev. Lett.* **107**, 096802 (2011).
8. K. Ishizaka, M. S. Bahramy, H. Murakawa, M. Sakano, T. Shimojima, T. Sonobe, K. Koizumi, S. Shin, H. Miyahara, A. Kimura, K. Miyamoto, T. Okuda, H. Namatame, M. Taniguchi, R. Arita, N. Nagaosa, K. Kobayashi, Y. Murakami, R. Kumai, Y. Kaneko, Y. Onose, Y. Tokura, Giant Rashba-type spin splitting in bulk BiTeI. *Nat. Mater.* **10**, 521–526 (2011).
9. J. Nitta, T. Akazaki, H. Takayanagi, T. Enoki, Gate control of spin-orbit interaction in an inverted $In_{0.53}Ga_{0.47}As/In_{0.52}Al_{0.48}As$ heterostructure. *Phys. Rev. Lett.* **78**, 1335–1338 (1997).
10. S. D. Stranks, H. J. Snaith, Metal-halide perovskites for photovoltaic and light-emitting devices. *Nat. Nanotechnol.* **10**, 391–402 (2015).
11. N.-G. Park, M. Grätzel, T. Miyasaka, K. Zhu, K. Emery, Towards stable and commercially available perovskite solar cells. *Nat. Energy* **1**, 16152 (2016).
12. Z. G. Yu, Effective-mass model and magneto-optical properties in hybrid perovskites. *Sci. Rep.* **6**, 28576 (2016).
13. M. Kepenekian, R. Robles, C. Katan, D. Sapori, L. Pedesseau, J. Even, Rashba and Dresselhaus effects in hybrid organic–inorganic perovskites: From basics to devices. *ACS Nano* **9**, 11557–11567 (2015).
14. C. Zhang, D. Sun, C.-X. Sheng, Y. X. Zhai, K. Mielczarek, A. Zakhidov, Z. V. Vardeny, Magnetic field effects in hybrid perovskite devices. *Nat. Phys.* **11**, 427–434 (2015).
15. Y.-C. Hsiao, T. Wu, M. Li, B. Hu, Magneto-optical studies on spin-dependent charge recombination and dissociation in perovskite solar cells. *Adv. Mater.* **27**, 2899–2906 (2015).
16. H. Tsai, W. Nie, J.-C. Blancon, C. C. Stoumpos, R. Asadpour, B. Harutyunyan, A. J. Neukirch, R. Verduzco, J. J. Crochet, S. Tretiak, L. Pedesseau, J. Even, M. A. Alam, G. Gupta, J. Lou, P. M. Ajayan, M. J. Bedzyk, M. G. Kanatzidis, A. D. Mohite, High-efficiency two-dimensional Ruddlesden–Popper perovskite solar cells. *Nature* **536**, 312–316 (2016).
17. D. H. Cao, C. C. Stoumpos, O. K. Farha, J. T. Hupp, M. G. Kanatzidis, 2D homologous perovskites as light-absorbing materials for solar cell applications. *J. Am. Chem. Soc.* **137**, 7843–7850 (2015).
18. D. Giovanni, W. K. Chong, H. A. Dewi, K. Thirumal, I. Neogi, R. Ramesh, S. Mhaisalkar, N. Mathews, T. C. Sum, Tunable room-temperature spin-selective optical Stark effect in solution-processed layered halide perovskites. *Sci. Adv.* **2**, e1600477 (2016).
19. J.-i. Fujisawa, T. Ishihara, Excitons and biexcitons bound to a positive ion in a bismuth-doped inorganic-organic layered lead iodide semiconductor. *Phys. Rev. B* **70**, 205330 (2004).
20. X. Hong, T. Ishihara, A. V. Nurmikko, Dielectric confinement effect on excitons in PbI_4-based layered semiconductors. *Phys. Rev. B* **45**, 6961–6964 (1992).
21. L. Sebastian, G. Weiser, One-dimensional wide energy bands in a polydiacetylene revealed by electroreflectance. *Phys. Rev. Lett.* **46**, 1156–1159 (1981).
22. M. E. Ziffer, J. C. Mohammed, D. S. Ginger, Electroabsorption spectroscopy measurements of the exciton binding energy, electron–hole reduced effective mass, and band gap in the perovskite $CH_3NH_3PbI_3$. *ACS Photonics* **3**, 1060–1068 (2016).
23. O. Yaffe, A. Chernikov, Z. M. Norman, Y. Zhong, A. Velauthapillai, A. van der Zande, J. S. Owen, T. F. Heinz, Excitons in ultrathin organic-inorganic perovskite crystals. *Phys. Rev. B* **92**, 045414 (2015).
24. J. Bordas, E. A. Davis, The excitons at the band edge of PbI_2. *Solid State Commun.* **12**, 717–720 (1973).
25. Y. Yacoby, Electric-field-induced indirect optical absorption in solids and the fine structure of the stark splitting. *Phys. Rev.* **140**, A263–A270 (1965).
26. D. E. Aspnes, Electric field effects on the dielectric constant of solids. *Phys. Rev.* **153**, 972–982 (1967).
27. C. Sheng, C. Zhang, Y. Zhai, K. Mielczarek, W. Wang, W. Ma, A. Zakhidov, Z. V. Vardeny, Exciton versus free carrier photogeneration in organometal trihalide perovskites probed by broadband ultrafast polarization memory dynamics. *Phys. Rev. Lett.* **114**, 116601 (2015).
28. G. S. Kanner, S. Frolov, Z. V. Vardeny, Detection of electronic excited states in conjugated polymers by picosecond transient strain spectroscopy. *Phys. Rev. Lett.* **74**, 1685–1688 (1995).
29. K. Abdel-Baki, F. Boitier, H. Diab, G. Lanty, K. Jemli, F. Lédée, D. Garrot, E. Deleporte, J. S. Lauret, Exciton dynamics and non-linearities in two-dimensional hybrid organic perovskites. *J. Appl. Phys.* **119**, 064301 (2016).
30. R. A. Kaindl, M. A. Carnahan, D. Hägele, R. Lövenich, D. S. Chemla, Ultrafast terahertz probes of transient conducting and insulating phases in an electron–hole gas. *Nature* **423**, 734–738 (2003).
31. C.-X. Sheng, Y. Zhai, U. Huynh, C. Zhang, Z. V. Vardeny, Ultrafast photomodulation spectroscopy of π-conjugated polymers, nanotubes and organometal trihalide perovskites: A comparison. *Synth. Met.* **216**, 31–39 (2016).
32. M. Fox, *Optical Properties of Solids* (Oxford Univ. Press, 2001).
33. D. Niesner, M. Wilhelm, I. Levchuk, A. Osvet, S. Shrestha, M. Batentschuk, C. Brabec, T. Fauster, Giant Rashba splitting in $CH_3NH_3PbBr_3$ organic–inorganic perovskite. *Phys. Rev. Lett.* **117**, 126401 (2016).
34. G. Bastard, *Wave Mechanics Applied to Semiconductor Heterostructures* (Les Edition de Physique, 1988).
35. M. Olszakier, E. Ehrenfreund, E. Cohen, Determination of the extension of the heavy-hole wave function in GaAs by photomodulation spectroscopy. *Phys. Rev. B* **43**, 9350 (1991).
36. J. Even, L. Pedesseau, J.-M. Jancu, C. Katan, Importance of spin-orbit coupling in hybrid organic/inorganic perovskites for photovoltaic applications. *J. Phys. Chem. Lett.* **4**, 2999–3005 (2013).
37. J. Calabrese, N. L. Jones, R. L. Harlow, N. Herron, D. L. Thorn, Y. Wang, Preparation and characterization of layered lead halide compounds. *J. Am. Chem. Soc.* **113**, 2328–2330 (1991).
38. T. Ishihara, J. Takahashi, T. Goto, Optical properties due to electronic transitions in two-dimensional semiconductors $(C_nH_{2n+1}NH_3)_2PbI_4$. *Phys. Rev. B Condens. Matter* **42**, 11099 (1990).

Acknowledgments: We are grateful to D. Sun (North Carolina State University) for the helpful discussions. **Funding:** The work at the University of Utah was supported by the U.S. Department of Energy Office of Science (grant DE-SC0014579). The film growth facility, C.Z., and S.B. were supported by the NSF Material Science and Engineering Center program at the University of Utah (grant DMR 1121252). E.E. acknowledges support from the Israel Science Foundation (grant no. 598/14). C.-X.S. acknowledges support from the National Science Foundation of China (grant no. 61574078) and the Fundamental Research Funds for the Central Universities (grant no. 30915011202). J.L. acknowledges support under the Cooperative Research Agreement between the University of Maryland and the National Institute of Standards and Technology Center for Nanoscale Science and Technology (award 70NANB14H209) through the University of Maryland. **Author contributions:** The project was planned by Z.V.V. Films were grown and characterized by C.Z. All of the measurements were conducted by Y.Z., S.B., and C.-X.S. The data analysis was performed by Z.V.V., C.-X.S., and E.E. The calculations were carried out by P.H. and J.L. The manuscript was prepared by Z.V.V., C.-X.S., and P.H. and discussed with all other authors. **Competing interests:** The authors declare that they have no competing interests. **Data and materials availability:** All data needed to evaluate the conclusions in the paper are present in the paper and/or the Supplementary Materials. Additional data related to this paper may be requested from the authors.

Submitted 6 March 2017
Accepted 26 June 2017
Published 28 July 2017
10.1126/sciadv.1700704

Citation: Y. Zhai, S. Baniya, C. Zhang, J. Li, P. Haney, C.-X. Sheng, E. Ehrenfreund, Z. V. Vardeny, Giant Rashba splitting in 2D organic-inorganic halide perovskites measured by transient spectroscopies. *Sci. Adv.* **3**, e1700704 (2017).

Giant Rashba splitting in 2D organic-inorganic halide perovskites measured by transient spectroscopies

Yaxin Zhai, Sangita Baniya, Chuang Zhang, Junwen Li, Paul Haney, Chuan-Xiang Sheng, Eitan Ehrenfreund and Zeev Valy Vardeny

Sci Adv **3** (7), e1700704.
DOI: 10.1126/sciadv.1700704